Physica A 394 (2014) 110–123

Contents lists available at ScienceDirect

Physica A

journal homepage: www.elsevier.com/locate/physa

Ultra-relativistic nonthermal power-law ensembles: Cosmic-ray electrons and positron fraction

Roman Tomaschitz *

Department of Physics, Hiroshima University, 1-3-1 Kagami-yama, Higashi-Hiroshima 739-8526, Japan

HIGHLIGHTS

- Relativistic power-law densities admit a stable and extensive entropy functional.
- Positive heat capacities and compressibility ensure their thermodynamic stability.
- Quantization of nonthermal relativistic power-law ensembles in Fermi statistics.
- Spectral fitting of nonthermal plasmas with ultra-relativistic power-law densities.
- Entropy, temperature and chemical potential of the cosmic-ray electron/positron flux.

ARTICLE INFO

Article history:
Received 13 June 2013
Received in revised form 11 September 2013
Available online 9 October 2013

Keywords:
Nonthermal power-law distributions
Stability and extensivity of entropy
Quantization of stationary non-equilibrium ensembles
Hybrid quantum ensembles
Ultra-relativistic electron–positron plasma
Spectral fitting of a two-component plasma with power-law densities
Cosmic-ray electron/positron flux

ABSTRACT

Thermodynamically stable ultra-relativistic power-law distributions are employed to model the recently measured cosmic-ray electron flux and the positron fraction. The probability density of power-law ensembles in phase space is derived, as well as an extensive entropy functional. The phase–space measure is transformed into a spectral number density, parameterized with the Lorentz factor of the charges and quantized in Fermi statistics. Relativistic power-law ensembles admit positive heat capacities and compressibilities ensuring mechanical stability as well as positive root mean squares quantifying thermodynamic fluctuations. The wideband spectral fitting of dilute nonthermal electron–positron plasmas with ultra-relativistic power-law densities is explained.

1. Introduction

We study nonthermal power-law ensembles capable of reproducing the flux of ultra-relativistic particles [1–5] such as cosmic-ray electrons and positrons. In particular, we derive power-law distributions from empirical spectral fits which are thermodynamically and mechanically stable, admitting positive heat capacities and compressibilities. The entropy of power-law ensembles is shown to be an extensive variable, and the positivity of the root mean squares of thermodynamic variables is explicitly demonstrated, ensuring a negative second entropy differential $\mathrm{d}^2S \leq 0$ subject to the extremal condition $\mathrm{d}S = 0$.

The spectral number density of ultra-relativistic power-law ensembles admits a convenient parameterization by the Lorentz factor of the particles. We derive the classical number density from the phase–space probability measure, which is taken as the starting point for the quantization of classical power-law ensembles in Fermi statistics. We also briefly

* Tel.: +81 824 247361.
E-mail address: tom@geminga.org.

0378-4371/$ – see front matter
http://dx.doi.org/10.1016/j.physa.2013.09.068

outline the bosonic quantization of power-law densities as well as the fermionic counterpart to electromagnetic gray-body radiation, with Lorentz factors defined by group velocity in a dispersive spacetime. Hybrid quantum distributions interpolating between Fermi and Bose statistics are derived.

In Section 2, we give an overview of the power-law densities studied, including their partition function, the basic thermodynamic variables, their variances, the equations of state, and show thermodynamic stability. In Section 3, we study classical power-law densities in phase space, their probability density and entropy functional, fluctuations of internal energy, particle number and entropy, as well as the quantization of nonthermal power-law ensembles.

In Section 4, we discuss wideband spectral fitting with ultra-relativistic power-law densities. The power-law densities studied here are aimed at this purpose, being thermodynamically stable empirical distributions sufficiently general to reproduce the multiple spectral peaks of broadband spectra. We show how to extract temperature, fugacity and chemical potential, as well as the power-law amplitudes and exponents from the measured particle flux. We also discuss energy scales and conditions for the applicability of the classical limit of the distributions.

In Section 5, we perform a spectral fit to the cosmic-ray electron flux, employing an ultra-relativistic classical power-law density. We use GeV data sets collected with the PAMELA and Fermi satellites [6–8], extended into the low TeV region by an atmospheric Cherenkov array [9–11]. Based on the electronic number density (obtained from the spectral fit) and the recently measured positron fraction, we calculate the spectral number density of the cosmic-ray positron flux in the 1 GeV–3 TeV interval. Finally we estimate the specific energy and number densities, as well as temperature and entropy production of ultra-relativistic cosmic-ray electrons/positrons, which constitute a nonthermal two-component plasma, dilute and at high temperature. In Section 6, we present our conclusions.

2. Fermionic power-law distributions

2.1. General outline: spectral number density, partition function, entropy

Fermionic power-law ensembles are defined by the distributions (number densities)

$$\mathrm{d}\rho_{\mathrm{F}}(\gamma)=\frac{m^3 s}{2\pi^2(\hbar c)^3}\frac{\sqrt{\gamma^2-1}\gamma\,\mathrm{d}\gamma}{1+G(\gamma)\,\mathrm{e}^{\beta\gamma+\alpha}}, \tag{2.1}$$

parameterized by the Lorentz factor γ. The positive spectral function $G(\gamma)$ in the denominator is normalized as $G(1)=1$ and is to be determined from a spectral fit. The mass parameter m is a shortcut for the rest energy mc^2, so that $E=m\gamma$ is the particle energy, and s is the spin multiplicity. The dimensionless temperature parameter is $\beta=m/(k_{\mathrm{B}}T)$, with Boltzmann constant k_{B}. The dimensionless real fugacity parameter α is related to the chemical potential μ by $\alpha=-\beta\mu/m$, and $z=\mathrm{e}^{-\alpha}$ is the fugacity. We specify $G(\gamma)$ as a power-law ratio,

$$G(\gamma)=\gamma^{\delta}\frac{g(\gamma)}{g(1)},\qquad g(\gamma)=\frac{1+(\gamma/a_1)^{\sigma_1}+\cdots+(\gamma/a_n)^{\sigma_n}}{1+(\gamma/b_1)^{\rho_1}+\cdots+(\gamma/b_k)^{\rho_k}}, \tag{2.2}$$

where δ is a real power-law exponent. The amplitudes a_i, b_i defining $g(\gamma)$ are positive, and so are the exponents, $0<\sigma_1<\cdots<\sigma_n$ and $0<\rho_1<\cdots<\rho_k$. Empirical spectral functions of this type suitable to model multiple spectral peaks in wideband spectra have been suggested in Refs. [1–3], a specific choice of the ratio $g(\gamma)$ is worked out in Sections 4 and 5. Fermionic power-law ensembles with $g(\gamma)=1$ have been studied in Refs. [12–16], and thermodynamic stability of the ratios (2.2) is demonstrated in Section 2.2.

The particle number in a volume V is

$$N=-\frac{\partial}{\partial\alpha}\log Z_{\mathrm{F}}=V\int_{\gamma_{\mathrm{cut}}}^{\infty}\mathrm{d}\rho_{\mathrm{F}}(\gamma), \tag{2.3}$$

referring to particles with energies exceeding $E_{\mathrm{cut}}=m\gamma_{\mathrm{cut}}$, where $\gamma_{\mathrm{cut}}\geq 1$ is the cutoff Lorentz factor. The partition function Z_{F} is stated in (2.6). The ultra-relativistic limit of $\mathrm{d}\rho_{\mathrm{F}}(\gamma)$ is obtained by replacing $\sqrt{\gamma^2-1}\to\gamma$ in (2.1), which applies if $\gamma_{\mathrm{cut}}\gg 1$. The thermal Fermi–Dirac distribution is recovered with $\delta=0$, $g(\gamma)=1$ and $\gamma_{\mathrm{cut}}=1$ as the lower integration boundary of the partition function. Here, we study nonthermal averages with real power-law index δ and empirical spectral function $g(\gamma)$ extracted from spectral fits of measured flux densities.

The spectral number density (2.1) is based on the dispersion relation $p=(m/c)\sqrt{\gamma^2-1}$. The integration in momentum space is parameterized as $\mathrm{d}^3p=4\pi p^2p'(\gamma)\,\mathrm{d}\gamma$, so that the particle density (2.1) is compiled as

$$\mathrm{d}\rho_{\mathrm{F}}=\frac{s}{(2\pi\hbar)^3}\frac{\mathrm{d}^3p}{1+G(\gamma)\,\mathrm{e}^{\beta\gamma+\alpha}},\qquad \mathrm{d}^3p=\frac{4\pi m^3}{c^3}\sqrt{\gamma^2-1}\gamma\,\mathrm{d}\gamma. \tag{2.4}$$

Remark. We may consider a more general dispersion relation, $p=(m/c)\hat{\mu}\sqrt{\hat{\varepsilon}^2\gamma^2-1}$, with energy-dependent dimensionless permeabilities $\hat{\varepsilon}(\gamma)$ and $\hat{\mu}(\gamma)$ resulting in a dispersive power-law density, a massive counterpart to photonic gray-body radiation. The integration in (2.3) is then over intervals in which the radicand of $p(\gamma)$ is positive, and the normalization is done with the smallest possible Lorentz factor, $g(\gamma_{\min})$ instead of $g(1)$. We still have $\gamma=E/m$, and the Lorentz factor γ can be parameterized by group velocity via $m/\upsilon=\mathrm{d}p/\mathrm{d}\gamma$. Here, we use vacuum permeabilities, $\hat{\varepsilon}=\hat{\mu}=1$.

The internal energy (total energy of particles with Lorentz factor exceeding the lower threshold $\gamma_{\rm cut}$) is

$$U = -m\frac{\partial}{\partial\beta}\log Z_{\rm F} = mV\int_{\gamma_{\rm cut}}^{\infty}\gamma\,{\rm d}\rho_{\rm F}(\gamma), \tag{2.5}$$

so that the spectral energy density can be identified as $m\gamma\,{\rm d}\rho_{\rm F}(\gamma)$. The grand partition function reads, cf. (2.3) and (2.5),

$$\log Z_{\rm F} = \frac{Vm^3s}{2\pi^2(\hbar c)^3}\int_{\gamma_{\rm cut}}^{\infty}\log\left(1+\frac{{\rm e}^{-\beta\gamma-\alpha}}{G(\gamma)}\right)\sqrt{\gamma^2-1}\gamma\,{\rm d}\gamma. \tag{2.6}$$

Entropy is defined as extensive quantity like in thermal averages,

$$S(\beta,\alpha,V) = k_{\rm B}\left(\log Z_{\rm F}+\beta\frac{U}{m}+\alpha N\right). \tag{2.7}$$

On introducing specific densities for the extensive variables, S/V, U/V and N/V, the volume factor drops out in (2.7), since $\log Z_{\rm F}\propto V$, so that S is homogeneous. We can also replace the partition function in (2.7) by the pressure variable P, $\log Z_{\rm F} = PV\beta/m$.

The classical limit of the partition function (2.6) is obtained by expanding the logarithm,

$$\log Z_{\rm B}(\beta,\alpha,V) = V\int_{\gamma_{\rm cut}}^{\infty}{\rm d}\rho_{\rm B}(\gamma), \tag{2.8}$$

where ${\rm d}\rho_{\rm B}$ is the Boltzmann power-law density

$${\rm d}\rho_{\rm B}(\gamma) = \frac{m^3s}{2\pi^2(\hbar c)^3}\frac{g(1)}{g(\gamma)}\,{\rm e}^{-\beta\gamma-\alpha}\gamma^{1-\delta}\sqrt{\gamma^2-1}\,{\rm d}\gamma, \tag{2.9}$$

which is the classical limit of the spectral number density ${\rm d}\rho_{\rm F}$ in (2.1) and (2.2), apparently valid for $G(\gamma)\,{\rm e}^{\beta\gamma+\alpha}\gg 1$. High- and low-temperature expansions of classical power-law ensembles based on ${\rm d}\rho_{\rm B}$ in (2.9) with $g(\gamma)=1$ and $s=1$ can be found in Ref. [12].

The spectral density of the non-relativistic Fermi gas,

$${\rm d}\rho_{\rm F,nr}(\upsilon) = \frac{m^3s}{(\hbar c)^3 2\pi^2}\frac{\upsilon^2\,{\rm d}\upsilon}{1+{\rm e}^{\beta\upsilon^2/2+\alpha_0}}, \tag{2.10}$$

is recovered by expanding the Lorentz factor in the power-law density (2.1) as $\gamma=(1-\upsilon^2)^{-1/2}\approx 1+\upsilon^2/2$. The power-law factor $G(\gamma)$ does not enter in leading order in the υ^2 expansion, $G(\gamma)\sim 1$, and the rest mass can be absorbed in the fugacity, $z_0={\rm e}^{-\alpha_0}$, $\alpha_0=\alpha+\beta$. The non-relativistic chemical potential μ_0 is obtained by subtracting the rest mass from the relativistic potential, $\mu_0=-\alpha_0 m/\beta=\mu-m$. We find the particle count

$$N = -\frac{\partial}{\partial\alpha_0}\log Z_{\rm F,nr}(\beta,\alpha_0,V) = V\int_0^{\infty}{\rm d}\rho_{\rm F,nr}(\upsilon) \tag{2.11}$$

and the partition function

$$\log Z_{\rm F,nr} = \frac{Vm^3s}{(\hbar c)^3 2\pi^2}\int_0^{\infty}\log(1+{\rm e}^{-\beta\upsilon^2/2-\alpha_0})\upsilon^2\,{\rm d}\upsilon. \tag{2.12}$$

The velocity parameter υ is dimensionless, measured in units of c. The classical Maxwell distribution is obtained by expanding the denominator of (2.10) and the logarithm in (2.12). The non-relativistic limit of the power-law densities (2.1) is always a thermal distribution, since $G(\gamma)\sim 1$ in leading order.

2.2. Thermodynamic stability: positivity of specific heat and compressibility

For the remainder of this section, we consider the classical limit based on the partition function (2.8) and density ${\rm d}\rho_{\rm B}$ in (2.9). In this limit, we can identify $N=\log Z_{\rm B}$, cf. (2.3), so that $P=mN/(\beta V)$ is the thermal equation of state, cf. after (2.7). We may then explicitly solve (2.8) for $\alpha(\beta,N/V)$ and substitute this into the classical limit of the internal energy (2.5) and entropy (2.7) to obtain the $U(\beta,N,V)$ and $S(\beta,N,V)$ representations thereof:

$$\alpha(\beta,N/V) = \log\left(\frac{m^3s}{2\pi^2(\hbar c)^3}\frac{V}{N}K(\beta)\right), \tag{2.13}$$

where we use the shortcut

$$K(\beta) = g(1)\int_{\gamma_{\rm cut}}^{\infty}{\rm e}^{-\beta\gamma}\frac{\gamma^{1-\delta}}{g(\gamma)}\sqrt{\gamma^2-1}\,{\rm d}\gamma. \tag{2.14}$$

$g(\gamma)$ is the power-law ratio in (2.2). We write $N(\beta,\alpha,V)$ in (2.3) and $U(\beta,\alpha,V)$ in (2.5) as

$$N = \mathrm{e}^{-\alpha}\frac{Vm^3 s}{2\pi^2(\hbar c)^3}K(\beta), \qquad U = -\frac{Vm^4 s}{2\pi^2(\hbar c)^3}\,\mathrm{e}^{-\alpha}K_{,\beta}, \tag{2.15}$$

which gives the caloric equation of state by eliminating the fugacity,

$$U(\beta,N) = -mN(\log K)_{,\beta}. \tag{2.16}$$

As $U \propto N$, we find equipartition of energy even at stationary non-equilibrium. In the low-temperature regime, the kinetic particle energy of an ideal gas is recovered as leading order in a $1/\beta$ expansion, $U/N - m \sim (3/2)m/\beta$.

The entropy (2.7) reads in the $S(\beta,N,V)$ representation

$$S = k_{\mathrm{B}}N\left[1 - \beta(\log K)_{,\beta} + \log K(\beta) + \log\frac{m^3 sV}{2\pi^2(\hbar c)^3 N}\right], \tag{2.17}$$

with integral $K(\beta)$ in (2.14). The free energy $F(\beta,N,V)$ is found via (2.16) and (2.17), $F = U - mS/(k_{\mathrm{B}}\beta)$. The isothermal compressibility follows from the thermal equation of state,

$$\kappa_T = -\frac{1}{V}V_{,P}(\beta,P,N) = \frac{1}{P}, \tag{2.18}$$

and the adiabatic compressibility is calculated via the heat capacities, $\kappa_S = \kappa_T C_V/C_P$. Thus, if $0 \le C_V \le C_P$ is satisfied, this also implies mechanical stability $0 \le \kappa_S \le \kappa_T$. The isochoric heat capacity is

$$C_V = TS_{,T}(\beta,N,V) = U_{,T}(\beta,N) = k_{\mathrm{B}}N\beta^2(\log K)_{,\beta,\beta}, \tag{2.19}$$

and the isobaric specific heat reads

$$C_P = TS_{,T}(\beta,N,P) = C_V + k_{\mathrm{B}}N = k_{\mathrm{B}}N(1+\beta^2(\log K)_{,\beta,\beta}). \tag{2.20}$$

Thus the stability criteria to guarantee $\mathrm{d}^2S \le 0$ are satisfied, since $(\log K)_{,\beta,\beta} \ge 0$ holds according to the Schwarz inequality $(K_{,\beta})^2 \le KK_{,\beta,\beta}$.

Stability implies well-defined positive standard deviations of the thermodynamic variables. Temperature fluctuations are determined by the isochoric specific heat,

$$\langle(\Delta T)^2\rangle = \frac{k_{\mathrm{B}}T^2}{C_V} = \frac{m^2}{k_{\mathrm{B}}^2\beta^4 N}\frac{1}{(\log K)_{,\beta,\beta}}, \tag{2.21}$$

and pressure fluctuations by the adiabatic compressibility,

$$\langle(\Delta P)^2\rangle = \frac{k_{\mathrm{B}}T}{V\kappa_S} = \frac{P^2}{N}\left(1 + \frac{1}{\beta^2(\log K)_{,\beta,\beta}}\right), \tag{2.22}$$

where we can use the thermal equation of state to obtain the (β,N,V) representation thereof. Relative fluctuations such as $\sqrt{\langle(\Delta P)^2\rangle}/P$ scale with $N^{-1/2}$. The variance of the chemical potential can be assembled as

$$\langle(\Delta\mu)^2\rangle = \frac{m^2}{\beta^2 N}\left(1 + \left(\alpha + \frac{\beta}{m}\frac{U}{N}\right)^2\frac{k_{\mathrm{B}}N}{C_V}\right), \tag{2.23}$$

with α in (2.13), U in (2.16) and C_V in (2.19) substituted. The variances of the extensive variables (internal energy, particle count and entropy) will be derived in phase space, cf. Section 3.2.

3. Power-law ensembles in phase space

3.1. Classical probability density

We give a probabilistic interpretation of the classical spectral number density $\mathrm{d}\rho_{\mathrm{B}}(\gamma)$ in (2.9). To this end, we consider the phase space of n particles with measure

$$\mathrm{d}^{3n}(p,q) = \frac{1}{(2\pi\hbar)^{3n}}\,\mathrm{d}^3p_1\,\mathrm{d}^3q_1\,\mathrm{d}^3p_2\,\mathrm{d}^3q_2\cdots\mathrm{d}^3p_n\,\mathrm{d}^3q_n,$$
$$\mathrm{d}^3p_i = \frac{4\pi m^3}{c^3}\sqrt{\gamma_i^2-1}\,\gamma_i\,\mathrm{d}\gamma_i, \tag{3.1}$$

where the d^3q_i integration is over a volume V, and the $\mathrm{d}\gamma_i$ integrations range in the interval $\gamma_{\rm cut} \le \gamma_i \le \infty$, cf. after (2.3). The angular integration over the solid angle $\mathrm{d}\Omega$ has been carried out and gives the factor 4π. The scale factor $(2\pi\hbar)^{3n}$ renders the measure dimensionless. The probability density on the n-particle states factorizes as

$$f_n(p,q) = \frac{s^n}{n!} b_n(p,q) h_n(p,q),$$
$$b_n(p,q) = \exp\left(-\xi - \beta\sum_{i=1}^n \gamma_i - \alpha n\right), \qquad h_n(p,q) = \exp\left(-\sum_{i=1}^n \log G(\gamma_i)\right). \tag{3.2}$$

The factor $1/n!$ accounts for indistinguishability and the positive integer s for spin multiplicity. The normalization factor ξ included in the weight $b_n(p,q)$ is found by summation over the n-particle subspaces,

$$\sum_{n=0}^\infty \int f_n(p,q)\,\mathrm{d}^{3n}(p,q) = 1. \tag{3.3}$$

The integrals in (3.3) factorize,

$$\int f_n(p,q)\,\mathrm{d}^{3n}(p,q) = \mathrm{e}^{-\xi}\frac{1}{n!}\left(V\frac{4\pi s m^3}{(2\pi\hbar c)^3}\,\mathrm{e}^{-\alpha}\int_{\gamma_{\rm cut}}^\infty \frac{\mathrm{e}^{-\beta\gamma}}{G(\gamma)}\sqrt{\gamma^2-1}\,\gamma\,\mathrm{d}\gamma\right)^n. \tag{3.4}$$

Substituting this into (3.3), we obtain the normalization constant $\xi = \log Z_{\rm B}$ as stated in (2.8).

3.2. Fluctuations and entropy in phase space

The normalization condition (3.3) can be written as

$$\sum_{n=0}^\infty \frac{s^n}{n!}\int \exp\left(-\beta\sum_{i=1}^n \gamma_i - \alpha n\right) h_n(p,q)\,\mathrm{d}^{3n}(p,q) = Z_{\rm B}(\beta,\alpha,V). \tag{3.5}$$

Accordingly, cf. (3.3),

$$\sum_{n=0}^\infty \int n f_n(p,q)\,\mathrm{d}^{3n}(p,q) = -(\log Z_{\rm B})_{,\alpha} = \langle n\rangle,$$
$$\sum_{n=0}^\infty \int n^2 f_n(p,q)\,\mathrm{d}^{3n}(p,q) = \frac{Z_{{\rm B},\alpha,\alpha}}{Z_{\rm B}} = \langle n^2\rangle. \tag{3.6}$$

We use the shortcut $\xi = \log Z_{\rm B}$ and the general identity $Z_{{\rm B},\beta,\alpha}/Z_{\rm B} = \xi_{,\beta,\alpha} + \xi_{,\beta}\xi_{,\alpha}$ as well as the special properties $\xi_{,\alpha} = -\xi$ and $N = \xi(\beta,\alpha,V)$. Thus, $\langle n\rangle = N$ and $\langle n^2\rangle = N(N+1)$, keeping the volume V constant in contrast to the fluctuating particle number N.

Analogously, we find the energy averages

$$\sum_{n=0}^\infty \int \left(\sum_{i=1}^n \gamma_i\right) f_n(p,q)\,\mathrm{d}^{3n}(p,q) = -(\log Z_{\rm B})_{,\beta} = \frac{1}{m}\langle u\rangle,$$
$$\sum_{n=0}^\infty \int \left(\sum_{i=1}^n \gamma_i\right)^2 f_n(p,q)\,\mathrm{d}^{3n}(p,q) = \frac{Z_{{\rm B},\beta,\beta}}{Z_{\rm B}} = \frac{1}{m^2}\langle u^2\rangle, \tag{3.7}$$

with random variable $u = m\sum_{i=1}^n \gamma_i$. Since $U(\beta,\alpha,V) = -m\xi_{,\beta}$, we can identify $\langle u\rangle = U$ and $\langle u^2\rangle = -mU_{,\beta}(\beta,\alpha,V) + U^2$. Internal energy and particle count are correlated as

$$\sum_{n=0}^\infty \int \left(\sum_{i=1}^n \gamma_i\right) n f_n(p,q)\,\mathrm{d}^{3n}(p,q) = \frac{Z_{{\rm B},\beta,\alpha}}{Z_{\rm B}} = \frac{1}{m}\langle un\rangle, \tag{3.8}$$

so that $\langle un\rangle = (1+N)U$. The standard deviations are readily assembled with the expectation values (3.6)–(3.8). Defining $\Delta n = n - \langle n\rangle$, etc., we find the covariance matrix elements as

$$\langle(\Delta n)^2\rangle = \langle n^2\rangle - \langle n\rangle^2 = N,$$
$$\langle(\Delta u)^2\rangle = \langle u^2\rangle - \langle u\rangle^2 = -mU_{,\beta}(\beta,\alpha,V),$$
$$\langle \Delta u\Delta n\rangle = \langle un\rangle - \langle u\rangle\langle n\rangle = U. \tag{3.9}$$

The grand canonical energy variance can be written as, cf. (2.16) and (2.19),

$$\langle(\Delta u)^2\rangle = m^2 N\frac{K_{,\beta,\beta}}{K} = \frac{m^2 C_V}{\beta^2 k_{\rm B}} + \frac{U^2}{N}, \tag{3.10}$$

where we used the identities

$$U_{,\beta}(\beta,\alpha,V) = U_{,\beta}(\beta,N) - \frac{U^2}{mN}, \qquad U_{,\beta}(\beta,N) = -\frac{mC_V}{k_{\rm B}\beta^2}. \tag{3.11}$$

The entropy functional in phase space is defined with the factorized probability density (3.2),

$$S = -k_{\rm B}\sum_{n=0}^{\infty}\frac{s^n}{n!}\int h_n(p,q)b_n(p,q)\log b_n(p,q)\,{\rm d}^{3n}(p,q). \tag{3.12}$$

Thus,

$$S(\beta,\alpha,V) = k_{\rm B}\sum_{n=0}^{\infty}\int f_n(p,q)\left(\xi+\beta\sum_{i=1}^{n}\gamma_i+\alpha n\right){\rm d}^{3n}(p,q), \tag{3.13}$$

where $\xi = \log Z_{\rm B}$ is the classical partition function (2.8). This is identical to the entropy $S(\beta,\alpha,V)$ stated in (2.7), according to the averages (3.5) and (3.7) and the normalization (3.3). We regard (3.13) as the expectation value of $s = k_{\rm B}\left(\xi+\beta\sum_{i=1}^{n}\gamma_i+\alpha n\right)$, $S = \langle s\rangle$, and use the correlations (3.9) to assemble $\langle s^2\rangle$ and the entropy variance

$$\langle(\Delta s)^2\rangle = \langle s^2\rangle - \langle s\rangle^2 = k_{\rm B}C_V + k_{\rm B}^2 N\left(\alpha+\frac{\beta}{m}\frac{U}{N}\right)^2. \tag{3.14}$$

Here, we can substitute $\alpha(\beta,N/V)$ in (2.13), $U(\beta,N)$ in (2.16) and $C_V(\beta,N)$ in (2.19) to obtain the (T,N,V) representation of the fluctuations. Alternatively, we may obtain the entropy fluctuations by making use of error propagation. To this end, we employ the $S(U,N,V)$ representation, obtained by substituting $\alpha=\alpha(U,N,V)$, $\beta=\beta(U,N,V)$ (implicitly defined by (2.3) and (2.5)) into (2.7). The entropy variance (3.14) is recovered via

$$\langle(\Delta s)^2\rangle = (S_{,U})^2\langle(\Delta u)^2\rangle + (S_{,N})^2\langle(\Delta n)^2\rangle + 2S_{,U}S_{,N}\langle\Delta u\Delta n\rangle, \tag{3.15}$$

by substituting the identities $S_{,U} = k_{\rm B}\beta/m$, $S_{,N} = k_{\rm B}\alpha$ and the covariance matrix (3.9).

3.3. Quantized power-law distributions

The partition function (2.6) is obtained via a trace calculation in fermionic occupation number representation,

$$Z_{\rm F} = {\rm Tr}[\exp(-\beta\hat H - \alpha\hat N - \hat Q)]. \tag{3.16}$$

A basis $|n\rangle$ for the occupation number representation of the fermionic creation and annihilation operators $b_{\mathbf k}^{(+)}$ (labeled by the wave vector $\mathbf k$ of the modes) can be found in Ref. [17]. The particle number operator is $\hat N = \sum_{|\mathbf k|\geq k_{\rm cut}}\hat N_{\mathbf k}$, where $\hat N_{\mathbf k} = b_{\mathbf k}^+ b_{\mathbf k}$. The energy operator is $\hat H = \sum_{|\mathbf k|\geq k_{\rm cut}}\hat H_{\mathbf k}$, where $\hat H_{\mathbf k} = \gamma_{\mathbf k}\hat N_{\mathbf k}$. The power-law weight factor $h_n(p,q)$ of the classical probability density in (3.2) is quantized as $\exp(-\hat Q)$, $\hat Q = \sum_{|\mathbf k|\geq k_{\rm cut}}\hat Q_{\mathbf k}$, where $\hat Q_{\mathbf k} = (\log G(\gamma_{\mathbf k}))\hat N_{\mathbf k}$. The energy operator $\hat H$ is dimensionless, rescaled with the particle mass. $\gamma_{\mathbf k} = \hbar\omega_{\mathbf k}/m$ is the Lorentz factor parameterized with the wave vector, and m stands for mc^2. In the occupation number representation, the Hermitian number operators are diagonal, $\hat N_{\mathbf k}|n\rangle = n_{\mathbf k}|n\rangle$, and the fermionic occupation number $n_{\mathbf k}$ attached to a wave vector $\mathbf k$ can only take the values zero and one. (In the bosonic case sketched below, $n_{\mathbf k}$ ranges between zero and infinity.) We also note the dispersion relation $\hbar\omega_{\mathbf k} = \sqrt{(\hbar c)^2k^2+m^2}$, relating electron energy and wave number $k = p/\hbar = |\mathbf k|$. Finally, $k_{\rm cut} = (m/(\hbar c))\sqrt{\gamma_{\rm cut}^2-1}$ is the wave number of the lower energy threshold $\hbar\omega_{\rm cut} = m\gamma_{\rm cut}$. Integration over wave vectors is defined by ${\rm d}^3k = {\rm d}^3p/\hbar^3$, with the momentum-space measure ${\rm d}^3p$ parameterized by the Lorentz factor as in (3.1).

We employ box quantization, discretizing the wave vector as $\mathbf k = 2\pi\mathbf n/L$, so that $\mathbf k$ summations are taken over integer lattice points $\mathbf n$ in R^3, corresponding to periodic boundary conditions on a box of size $V = L^3$. By making use of $\hat N_{\mathbf k}|n\rangle = n_{\mathbf k}|n\rangle$, we can write trace (3.16) over the basis $|n\rangle$ as

$$\begin{aligned} Z_{\rm F} &= \sum_{n_{\mathbf k}=0,1}\exp\sum_{|\mathbf k|\geq k_{\rm cut}}(-\beta\gamma_{\mathbf k}-\alpha-\log G(\gamma_{\mathbf k}))n_{\mathbf k}\\ &= \prod_{|\mathbf k|\geq k_{\rm cut}}[1+\exp(-\beta\gamma_{\mathbf k}-\alpha-\log G(\gamma_{\mathbf k}))]. \end{aligned} \tag{3.17}$$

We thus find

$$\log Z_{\rm F} = \sum_{|\mathbf{k}|\geq k_{\rm cut}} \log\left(1+\frac{{\rm e}^{-\beta\gamma_{\mathbf{k}}-\alpha}}{G(\gamma_{\mathbf{k}})}\right). \tag{3.18}$$

The continuum limit $L\to\infty$ amounts to replacing the summation over the lattice wave vectors $\mathbf{k}$ by the integration $sV\int_{|\mathbf{k}|\geq k_{\rm cut}} {\rm d}^3k/(2\pi)^3$, where the factor s accounts for spin degeneracy,

$$\log Z_{\rm F} = \frac{sV}{(2\pi)^3}\int_{|\mathbf{k}|\geq k_{\rm cut}} \log\left(1+\frac{{\rm e}^{-\beta\gamma_{\mathbf{k}}-\alpha}}{G(\gamma_{\mathbf{k}})}\right){\rm d}^3k. \tag{3.19}$$

Introducing the Lorentz factor γ as integration variable, ${\rm d}^3k = 4\pi(m/(\hbar c))^3\sqrt{\gamma^2-1}\gamma{\rm d}\gamma$, we arrive at the partition function $\log Z_{\rm F}$ stated in (2.6).

We outline quantization of relativistic power-law ensembles in Bose–Einstein statistics [17–19]. In this case, the summation over the occupation numbers $n_{\mathbf{k}}$ in (3.17) extends to infinity,

$$Z_{\rm E} = \prod_{|\mathbf{k}|\geq k_{\rm cut}}\sum_{n=0}^{\infty}\exp[-n(\beta\gamma_{\mathbf{k}}+\alpha+\log G(\gamma_{\mathbf{k}}))], \tag{3.20}$$

which gives, cf. (3.18),

$$\log Z_{\rm E} = -\sum_{|\mathbf{k}|\geq k_{\rm cut}} \log\left(1-\frac{{\rm e}^{-\beta\gamma_{\mathbf{k}}-\alpha}}{G(\gamma_{\mathbf{k}})}\right). \tag{3.21}$$

Replacing the summation by the continuum limit, cf. (3.19), we arrive at the bosonic counterpart to the partition function (2.6),

$$\log Z_{\rm E} = -\frac{4\pi Vm^3s}{(2\pi\hbar c)^3}\int_{\gamma_{\rm cut}}^{\infty}\log\left(1-\frac{{\rm e}^{-\beta\gamma-\alpha}}{G(\gamma)}\right)\sqrt{\gamma^2-1}\gamma\,{\rm d}\gamma. \tag{3.22}$$

The bosonic spectral number density ${\rm d}\rho_{\rm E}(\gamma)$ can be identified via (2.3) and (3.22),

$$N = -\frac{\partial}{\partial\alpha}\log Z_{\rm E} = V\int_{\gamma_{\rm cut}}^{\infty}{\rm d}\rho_{\rm E}(\gamma), \tag{3.23}$$

$${\rm d}\rho_{\rm E}(\gamma) = \frac{4\pi m^3s}{(2\pi\hbar c)^3}\frac{\sqrt{\gamma^2-1}\gamma\,{\rm d}\gamma}{G(\gamma)\,{\rm e}^{\beta\gamma+\alpha}-1}, \tag{3.24}$$

which differs from the fermionic density ${\rm d}\rho_{\rm F}(\gamma)$ in (2.1) only by the minus sign in the denominator. s is a multiplicity index, and $G(\gamma)$ is the spectral function (2.2). In the bosonic case, the reciprocal spectral function $G^{-1}(\gamma)$ must be bounded, its maximum being attained at $\gamma_{\rm c}$. ($\gamma_{\rm c}$ can be infinite.) The fugacity $z={\rm e}^{-\alpha}$ is restricted by $z\leq z_{\rm c}=G(\gamma_{\rm c})$, so that the denominator in (3.24) is positive. The classical regime is $G(\gamma)\,{\rm e}^{\beta\gamma+\alpha}\gg 1$, whereas quantum condensation effects arise in the opposite limit, $G(\gamma)\,{\rm e}^{\beta\gamma+\alpha}\to 1$.

3.4. Hybrid quantum statistics

We briefly discuss hybrid distributions, in which the fermionic exclusion principle is softened to allow $N_{\rm id}$ identical particles labeled by the same wave vector $\mathbf{k}$. The partition function interpolating between Fermi and Bose statistics is found by extending the $n_{\mathbf{k}}$ summation in (3.17),

$$\begin{aligned} Z_{H(N_{id})} &= \sum_{n_{\mathbf{k}}=0}^{N_{\rm id}}\exp\sum_{|\mathbf{k}|\geq k_{\rm cut}}(-\beta\gamma_{\mathbf{k}}-\alpha-\log G(\gamma_{\mathbf{k}}))n_{\mathbf{k}} \\ &= \prod_{|\mathbf{k}|\geq k_{\rm cut}}\sum_{n=0}^{N_{\rm id}}\exp[-n(\beta\gamma_{\mathbf{k}}+\alpha+\log G(\gamma_{\mathbf{k}}))], \end{aligned} \tag{3.25}$$

where the allowed multiplicity of particles in identical states is an arbitrary positive integer $N_{\rm id}$. Summation of the finite geometric series in (3.25) gives

$$\log Z_{H(N_{\rm id})} = \sum_{|\mathbf{k}|\geq k_{\rm cut}}\log\frac{1-{\rm e}^{-(N_{\rm id}+1)(\beta\gamma_{\mathbf{k}}+\alpha+\log G(\gamma_{\mathbf{k}}))}}{1-{\rm e}^{-(\beta\gamma_{\mathbf{k}}+\alpha+\log G(\gamma_{\mathbf{k}}))}}. \tag{3.26}$$

Clearly, $\log Z_{H(N_{\rm id})} < \log Z_{H(N_{\rm id}+1)}$. Performing the continuum limit, cf. (3.19), we find

$$\log Z_{H(N_{\rm id})} = -\frac{4\pi Vm^3 s}{(2\pi\hbar c)^3}\int_{\gamma_{\rm cut}}^{\infty}\log\left(\frac{1-{\rm e}^{-(\beta\gamma+\alpha+\log G(\gamma))}}{1-{\rm e}^{-(N_{\rm id}+1)(\beta\gamma+\alpha+\log G(\gamma))}}\right)\sqrt{\gamma^2-1}\gamma\,{\rm d}\gamma. \tag{3.27}$$

The Fermi–Dirac and Bose–Einstein partitions $\log Z_{\rm F}$ in (2.6) and $\log Z_{\rm E}$ in (3.22) are recovered for $N_{\rm id}=1$ and $N_{\rm id}=\infty$, respectively. The spectral density ${\rm d}\rho_{H(N_{\rm id})}(\gamma)$ of a hybrid quantum ensemble of fixed multiplicity $N_{\rm id}$ can be identified as in (3.23) and (3.24) via the particle count,

$$N = -\frac{\partial}{\partial\alpha}\log Z_{H(N_{\rm id})} = V\int_{\gamma_{\rm cut}}^{\infty}{\rm d}\rho_{H(N_{\rm id})}(\gamma), \tag{3.28}$$

$${\rm d}\rho_{H(N_{\rm id})}(\gamma) = \frac{4\pi m^3 s}{(2\pi\hbar c)^3}\left(\frac{1}{{\rm e}^{\beta\gamma+\alpha+\log G(\gamma)}-1}-\frac{N_{\rm id}+1}{{\rm e}^{(N_{\rm id}+1)(\beta\gamma+\alpha+\log G(\gamma))}-1}\right)\sqrt{\gamma^2-1}\gamma\,{\rm d}\gamma. \tag{3.29}$$

The limit $N_{\rm id}\to\infty$ can be carried out in this representation of ${\rm d}\rho_{H(N_{\rm id})}(\gamma)$, provided that $\beta\gamma+\alpha+\log G(\gamma)>0$, cf. after (3.24). Even if this constraint is not met, the positivity of density (3.29) is obvious in the equivalent representation

$${\rm d}\rho_{H(N_{\rm id})}(\gamma) = \frac{4\pi m^3 s}{(2\pi\hbar c)^3}\left(\sum_{n=0}^{N_{\rm id}}{\rm e}^{n(\beta\gamma+\alpha+\log G(\gamma))}-(N_{\rm id}+1)\right)\frac{\sqrt{\gamma^2-1}\gamma\,{\rm d}\gamma}{{\rm e}^{(N_{\rm id}+1)(\beta\gamma+\alpha+\log G(\gamma))}-1}, \tag{3.30}$$

irrespective of the (finite) multiplicity $N_{\rm id}$ and the sign of exponent $\beta\gamma+\alpha+\log G(\gamma)$, and ${\rm d}\rho_{H(N_{\rm id})}(\gamma)$ stays finite when this exponent approaches zero. Alternatively, we may write the hybrid density (3.30) as

$${\rm d}\rho_{H(N_{\rm id})}(\gamma) = \frac{4\pi m^3 s}{(2\pi\hbar c)^3}\left(1-\frac{N_{\rm id}+1}{\sum_{n=0}^{N_{\rm id}}{\rm e}^{n(\beta\gamma+\alpha+\log G(\gamma))}}\right)\frac{\sqrt{\gamma^2-1}\gamma\,{\rm d}\gamma}{{\rm e}^{\beta\gamma+\alpha+\log G(\gamma)}-1}, \tag{3.31}$$

so that $0<{\rm d}\rho_{H(N_{\rm id})}(\gamma)<{\rm d}\rho_{H(N_{\rm id}+1)}(\gamma)$ is evident, cf. after (3.26), which holds for arbitrary real exponents $\beta\gamma+\alpha+\log G(\gamma)$. In contrast to the Bose–Einstein limit $N_{\rm id}=\infty$, there is no constraint on the fugacity parameter α resulting in a condensed phase, so that the reciprocal spectral function $1/G(\gamma)$ need not be bounded in hybrid statistics, even for high multiplicity, so long as $N_{\rm id}$ is finite.

Remarks. To check the stability of the above quantum densities, one starts with the high- and low-temperature asymptotics of the thermodynamic variables, which can be done analytically in leading order [13,14]. To check positivity of the specific heat and compressibility in the intermediate temperature regime, one has to specify the input parameters and study the cross-over numerically, in contrast to the classical variables discussed in Section 2.2. If positivity turns out to be violated for certain parameter ranges, the respective intervals have to be excluded. I also note that the power-law factor $G(\gamma)$ drops out in the non-relativistic limit also in the quantum distributions, and has a pronounced effect only for large Lorentz factors, so that their applicability is currently limited to astrophysical plasmas. Whether the hybrid densities (3.29) can be related to real systems remains to be seen. The spectral fits in Section 5 are performed with the classical density (2.9).

4. Nonthermal spectral fitting in the ultra-relativistic regime: How to set it up in practice

We write the spectral number density (2.1) as

$$\frac{{\rm d}\rho_{\rm F}(E)}{{\rm d}E} = \frac{m^2 s}{2\pi^2(\hbar c)^3}\frac{\sqrt{\gamma^2-1}\gamma}{1+\gamma^\delta g(\gamma)\,{\rm e}^{\beta\gamma+\alpha-\log g(1)}}, \tag{4.1}$$

with $\gamma=E/m$, where m stands for mc^2, and use dimensionless quantities: E and m in units of 10^{3d} GeV, where the factor 10^{3d} (usually with integer d) allows us to conveniently shift the energy scale. The units chosen for length, time and temperature are meter, second and Kelvin, so that $\hbar$ (10^{3d} GeV s) $\approx 6.582\times10^{-25-3d}$ and c (m/s) $\approx 2.998\times10^8$. Finally, $\beta=m/(k_{\rm B}T)$, with T (K) and $k_{\rm B}$ (10^{3d} GeV K^{-1}) $\approx 8.617\times10^{-14-3d}$. The contribution of the Coulomb interaction [20–22] to the partition function is negligible in the case of a dilute ultra-relativistic plasma at high temperature, since $e^2/(4\pi rk_{\rm B}T)\ll 1$, with interparticle distance $r=(N/V)^{-1/3}$ and fine-structure constant $e^2/(4\pi\hbar c)\approx 1/137$ (Heaviside–Lorentz system), cf. Table 1.

We rescale the temperature and fugacity parameters, as well as the amplitudes in the power-law ratio $g(\gamma)$ in (2.2),

$$\hat\beta=\frac{\beta}{m},\qquad \hat z=z\frac{m^\delta}{f_{\rm B}(m)},\qquad \hat a_i=a_i m,\qquad \hat b_i=b_i m, \tag{4.2}$$

Table 1
Thermodynamic parameters of the ultra-relativistic electron/positron distributions $\mathrm{d}\rho_\mathrm{B}/\mathrm{d}E$ in (5.3), extracted from the spectral fit of the electron flux $F_\mathrm{e}(E)$ in (5.4) and the positron flux $F_\mathrm{p}(E)$ in (5.7), cf. Figs. 1 and 2. N/V is the specific number density and U/V the specific energy density calculated via (4.12) with lower cutoff energy $E_\mathrm{cut} \approx 1$ GeV. Recorded are temperature T, fugacity z and chemical potential μ, cf. (4.11), as well as the specific entropy density S/V scaled with the Boltzmann constant, cf. (4.14). The entropy production is mainly due to the fugacity term in (4.14). For comparison, the specific entropy density of the cosmic microwave background is $2.9 \times 10^6 k_\mathrm{B}\,\mathrm{m}^{-3}$. The first row of the table refers to cosmic-ray electrons with energies above 1 GeV (lower energy threshold of the observed flux), the second to positrons.

	N/V (m^{-3})	U/V ($\mathrm{GeV\,m}^{-3}$)	$k_\mathrm{B}T$ (GeV)	$\log z$	μ (GeV)	$S/(k_\mathrm{B}V)$ (m^{-3})
e^-	1.8×10^{-6}	5.0×10^{-6}	1.0×10^3	-96.8	-9.7×10^4	1.8×10^{-4}
e^+	1.3×10^{-7}	3.4×10^{-7}	7.4×10^2	-95.3	-7.1×10^4	1.3×10^{-5}

where $f_\mathrm{B}(E) = g^{-1}(E/m)$ denotes the reparameterized reciprocal power-law ratio (2.2),

$$f_\mathrm{B}(E) = \frac{1}{g(E/m)} = \frac{1 + (E/\hat{b}_1)^{\rho_1} + \cdots + (E/\hat{b}_k)^{\rho_k}}{1 + (E/\hat{a}_1)^{\sigma_1} + \cdots + (E/\hat{a}_n)^{\sigma_n}}. \tag{4.3}$$

If we use constant or dispersive permeabilities differing from 1, cf. the Remark after (2.4), we define the scaling function as $f_\mathrm{B}(E) = g^{-1}(E/E_\mathrm{min})$, $E_\mathrm{min} = m\gamma_\mathrm{min}$, where γ_min is the smallest Lorentz factor admissible in the dispersion relation. The fermionic spectral number density (4.1) reads in dimensionless quantities

$$\frac{\mathrm{d}\rho_\mathrm{F}(E)}{\mathrm{d}E}((10^{3d}\,\mathrm{GeV})^{-1}\,\mathrm{m}^{-3}) = \frac{s\hat{z}}{2\pi^2(\hbar c)^3}\frac{E^{2-\delta}f_\mathrm{B}(E)\,\mathrm{e}^{-\hat{\beta}E}}{1 + \hat{z}E^{-\delta}f_\mathrm{B}(E)\,\mathrm{e}^{-\hat{\beta}E}}\sqrt{1 - \frac{m^2}{E^2}}. \tag{4.4}$$

The classical number density $\mathrm{d}\rho_\mathrm{B}/\mathrm{d}E$ is obtained by approximating the denominator by 1.

The spectral flux density is found by multiplying the number density (4.4) with the group velocity,

$$\upsilon = \frac{\mathrm{d}E}{\mathrm{d}p} = c\frac{\sqrt{\gamma^2 - 1}}{\gamma} = c\sqrt{1 - \frac{m^2}{E^2}}. \tag{4.5}$$

The spectral flux density per steradian is thus

$$F(E) := \frac{\mathrm{d}\Phi_\mathrm{F}}{\mathrm{d}E\,\mathrm{d}\Omega} = \frac{c}{4\pi}\sqrt{1 - \frac{m^2}{E^2}}\frac{\mathrm{d}\rho_\mathrm{F}(E)}{\mathrm{d}E}, \tag{4.6}$$

where $\mathrm{d}\Omega$ is the solid angle increment and $\mathrm{d}\rho_\mathrm{F}/\mathrm{d}E$ the particle density (4.4). Density $F(E)$ is the spectral number flux; the spectral energy flux is obtained by rescaling $F(E)$ with E. To avoid steep spectral slopes in log–log plots, which tend to conceal the fine-structure, it is convenient to rescale $F(E)$ with a suitable power E^k, where k is usually integer. (We will use $k = 3$ in Section 5.) In dimensionless quantities, cf. (4.4) and (4.6),

$$E^kF(E)((10^{3d}\,\mathrm{GeV})^{k-1}\,\mathrm{m}^{-2}\,\mathrm{sr}^{-1}\,\mathrm{s}^{-1}) = \frac{\hat{y}E^{2+k-\delta}f_\mathrm{B}(E)\,\mathrm{e}^{-\hat{\beta}E}}{1 + \xi_0\hat{y}E^{-\delta}f_\mathrm{B}(E)\,\mathrm{e}^{-\hat{\beta}E}}\left(1 - \frac{m^2}{E^2}\right), \tag{4.7}$$

where we introduced the shortcuts, cf. (4.2),

$$\hat{y} = \hat{z}/\xi_0, \qquad \xi_0 = (2\pi\hbar)^3c^2/s. \tag{4.8}$$

s is the spin multiplicity. The classical flux $F_\mathrm{B}(E)$ (defined by the Boltzmann density $\mathrm{d}\rho_\mathrm{B}/\mathrm{d}E$ substituted in (4.6)) is found by dropping the ξ_0 term in the denominator of (4.7),

$$E^kF_\mathrm{B}(E) = \hat{y}E^{2+k-\delta}f_\mathrm{B}(E)\,\mathrm{e}^{-\hat{\beta}E}\left(1 - \frac{m^2}{E^2}\right). \tag{4.9}$$

In the ultra-relativistic regime, we can ignore the factor $1 - m^2/E^2$ as well; this limit will be used in the spectral fits in Section 5.

In a wideband fit, it is convenient to represent the spectral function $f_\mathrm{B}(E)$ in (4.9) by a series of power-law peaks [3],

$$\hat{y}E^{2+k-\delta}f_\mathrm{B}(E) = \sum_{i=1}^{m}\frac{(E/\hat{c}_i)^{\eta_i}}{1 + (E/\hat{d}_i)^{\kappa_i}}, \tag{4.10}$$

with positive amplitudes $\hat{c}_i$, $\hat{d}_i$ and real exponents η_i, κ_i (determining location, height and the two power-law slopes of each peak) to be extracted from the spectral fit. Once the exponents and amplitudes on the right-hand side of (4.10) are known, the power-law ratio $f_\mathrm{B}(E)$ in (4.3) is unambiguously defined. The amplitude $\hat{y}$ and the exponent $2 + k - \delta$ can readily be identified as well, by considering the limit $E \to 0$ in (4.10).

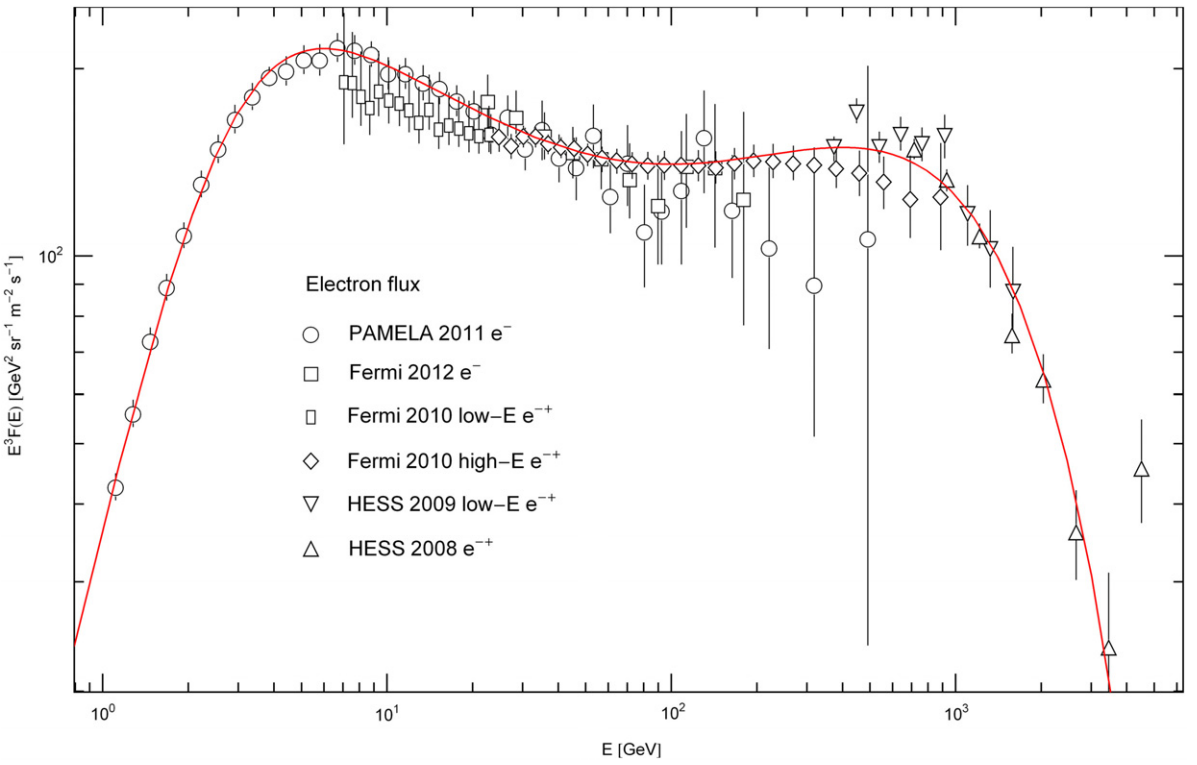

Fig. 1. Cosmic-ray electron flux. Data points from PAMELA 2011 (magnetic spectrometer combined with calorimeter for bremsstrahlung showers, pure electron flux) [6], Fermi LAT 2012 (Large Area pair-conversion γ-ray Telescope, pure electron flux) [7], Fermi LAT 2010 (combined electron–positron flux) [8], HESS 2009 (High-Energy Stereoscopic System, an imaging atmospheric Cherenkov telescope, low-energy component of combined electron–positron flux) [10], and HESS 2008 (high-energy component of combined electron–positron flux) [11]. The low-energy Fermi LAT 2010 data are not included in the fit, as they are not compatible with the overlapping PAMELA flux, which has smaller error bars in this region. The fit does not discriminate between pure electron and combined electron–positron data points. (The Fermi 2012 pure electron data are quite comparable to the Fermi 2010 combined electron–positron data, in fact intersecting them. The Fermi 2010 low-energy flux is a combined electron–positron flux, whereas the overlapping PAMELA flux has a noticeably higher intensity even though it is a pure electron flux.) The solid curve is a plot of the ultra-relativistic nonthermal electron flux $F_e(E)$ (spectral number-flux density, scaled with E^3 in the figure) stated in (5.4); the fitting parameters in (5.1) and (5.2) can be read off from the analytic representation of $E^3F_e(E)$ in (5.4). The thermodynamic parameters of the electronic power-law distribution (5.3) generating the depicted flux density are listed in Table 1.

Remark. The individual spectral components of nonthermal high-energy spectra are typically composed of a power-law ascent, followed by a slightly curved descending power-law slope due to an exponential cutoff [15,16]. Power-law slopes are linear in log – log plots, clearly distinguishable from curved exponential cutoffs, and wideband spectra can readily be assembled with them. The power-law slopes are often blurred due to overlapping spectral peaks. The spectral function (4.10) models a sequence of such spectral peaks. Given that spectral fits are usually performed in double logarithmic representation, power-law ratios of type (2.2) and (4.3) seem to be sufficiently general, although more complicated spectral functions have been considered [2]. The spectral functions (2.2) are constant for small Lorentz factors, $g(\gamma \to 1) \sim 1$, and have a power-law shape in the opposite limit, $g(\gamma \to \infty) \propto \gamma^{\sigma_n-\rho_k}$. A different cross-over (other than in (2.2)) does not affect the thermodynamic stability, cf. Section 2.2, but if one replaces, for instance, the denominators in (4.10) by $(1+E/\hat{d}_i)^{\kappa_i}$, it would not be possible to fit the electron spectrum in Fig. 1.

The chemical potential $\mu = -\alpha/\hat{\beta}$, temperature and fugacity $z = \mathrm{e}^{-\alpha}$ can be extracted from the fitting parameters $\hat{\beta}$ and $\hat{y}$, cf. (4.2) and (4.8),

$$\mu(10^{3d}\ \mathrm{GeV}) = k_\mathrm{B}T\log z, \qquad k_\mathrm{B}T = \frac{1}{\hat{\beta}}, \qquad z = \xi_0\hat{y}\frac{f_\mathrm{B}(m)}{m^\delta}. \tag{4.11}$$

Here, $\xi_0 \approx 3.18\times 10^{-9(d+6)}(2/s)$, which becomes moderate on the 10^{-9} eV scale ($d = -6$), cf. (4.8) and after (4.1), and $m \approx 0.511\times 10^{-3(d+1)}$ for an electron/positron gas. The specific particle density N/V in (2.3) reads in dimensionless quantities

$$\frac{N}{V}(\mathrm{m}^{-3}) = \frac{4\pi}{c}\hat{y}\int_{E_\mathrm{cut}}^{\infty}\frac{f_\mathrm{B}(E)\sqrt{1-m^2/E^2}}{\xi_0\hat{y}f_\mathrm{B}(E)+E^\delta\,\mathrm{e}^{\hat{\beta}E}}E^2\,\mathrm{d}E, \tag{4.12}$$

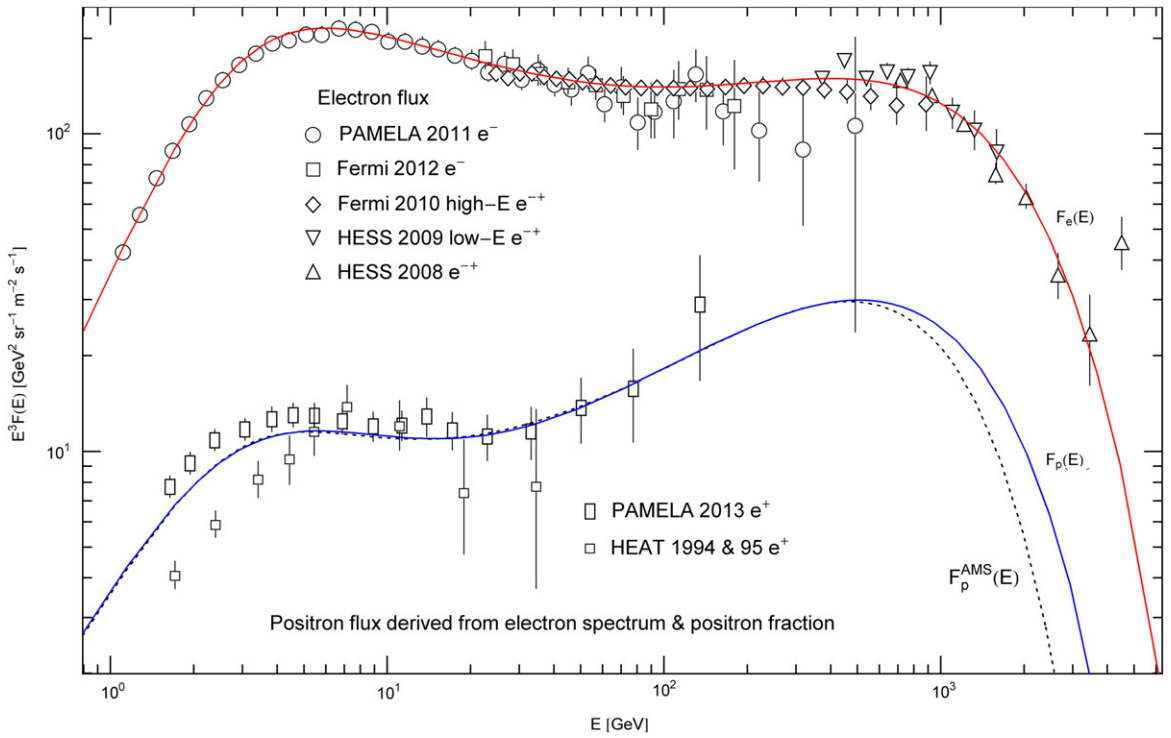

Fig. 2. Cosmic-ray positron spectrum inferred from the measured electron flux and the positron fraction. The electron flux $F_e(E)$ (upper solid curve, a plot of $E^3F_e(E)$ in (5.4)) is the same as in Fig. 1, on a compressed flux scale. The dotted curve labeled $F_p^{AMS}(E)$ is the positron flux (5.6) assembled from the depicted fit $F_e(E)$ of the electron flux and the analytic AMS fit $R_p^{AMS}(E)$ of the positron fraction [23] stated in (5.5). The AMS positron fraction $R_p^{AMS}(E)$ has been measured only up to 300 GeV, cf. Fig. 3, so that the dotted curve $F_p^{AMS}(E)$ above this energy is an extrapolation based on the analytic ratio $R_p^{AMS}(E)$ in (5.5). The solid curve $F_p(E)$ is the predicted positron flux stated in (5.7), obtained by approximating $F_p^{AMS}(E)$ below 300 GeV by a nonthermal power-law density analogous to the electronic flux density $F_e(E)$. The positronic fitting parameters can be read off from $E^3F_p(E)$ in (5.7), and the thermodynamic parameters of the positron flux are recorded in Table 1. The depicted positron data from PAMELA 2013 [24] and HEAT (High-Energy Antimatter Telescope, a balloon-born superconducting magnet spectrometer with calorimeter and scintillation counters attached) [29] have not been used in the derivation of the positronic flux density.

and the partition function (2.6),

$$\frac{\log Z_F}{V}(\mathrm{m}^{-3}) = \frac{4\pi}{c\xi_0}\int_{E_{\mathrm{cut}}}^{\infty} \log(1+\xi_0\hat{y}f_B(E)E^{-\delta}\,\mathrm{e}^{-\hat{\beta}E})\sqrt{1-\frac{m^2}{E^2}}E^2\,\mathrm{d}E, \tag{4.13}$$

where the lower cutoff energy is related to the Lorentz factor by $E_{\mathrm{cut}} = m\gamma_{\mathrm{cut}}$. The energy density U/V (10^{3d} GeV m^{-3}), cf. (2.5), is obtained by adding a factor E to the integrand in (4.12). (These integrals are numerically very tame.) The specific densities N/V and U/V become independent of the particle rest mass m in the ultra-relativistic regime $m^2/E_{\mathrm{cut}}^2 \ll 1$, since the roots in (4.12) and (4.13) can be dropped, so that the mass is completely absorbed in the fitting parameters. The classical limit of the particle density N/V is found by putting the $\xi_0\hat{y}f_B(E)$ term in the denominator of the integrand in (4.12) to zero. Since ξ_0 is extremely small on the GeV scale and the amplitude $\hat{y}$ (extracted from the spectral fit) turns out to be moderate, we can safely assume $\xi_0\hat{y}f_B(E) \ll E^\delta\,\mathrm{e}^{\hat{\beta}E}$ and use the classical limit. Expanding the logarithm in the partition function (4.13) in leading order in $\xi_0\hat{y}$, we recover $N = \log Z_B$, cf. before (2.13). The entropy density (2.7) can be assembled from the classical specific number and energy densities in (4.12),

$$\frac{1}{k_B}\frac{S}{V}(\mathrm{m}^{-3}) = (1-\log z)\frac{N}{V} + \frac{1}{k_BT}\frac{U}{V}, \tag{4.14}$$

where we have put $\alpha = -\log z$ in (2.7). Fugacity and temperature are extracted from the fitting parameters by way of (4.11). As mentioned, in the ultra-relativistic limit, we do not need to know the mass of the particles to calculate the specific particle and energy densities (4.12) from the spectral fit. However, the particle mass affects the entropy density via the fugacity, cf. (4.11), as the entropy depends on the zero point of the chemical potential. This zero point is determined by the normalization of the spectral function $G(\gamma)$ in (2.1) at $\gamma = 1$. We have chosen $G(1) = 1$, so that the chemical potential of the non-relativistic Fermi gas limit is recovered from the relativistic potential μ in (4.11) by subtraction of the rest mass, cf. after (2.10).

5. Spectral flux densities and thermodynamic parameters of cosmic-ray electrons/positrons

The spectral fits in Figs. 1 and 2 are performed with the classical ultra-relativistic flux density $F_{\rm B}(E)$ in (4.9) and the spectral function $f_{\rm B}(E)$ in (4.3). We employ a GeV energy scale ($d = 0$, cf. after (4.1)), and scale the flux density with E^3, cf. (4.9),

$$E^3F_{\rm B}(E)(\mathrm{GeV}^2\ \mathrm{m}^{-2}\ \mathrm{sr}^{-1}\ \mathrm{s}^{-1}) \sim \hat{y}E^{5-\delta}f_{\rm B}(E)\ \mathrm{e}^{-\hat{\beta}E}. \tag{5.1}$$

The spectral function is composed of two power-law peaks, cf. (4.3) and (4.10),

$$f_{\rm B}(E) = \frac{1+(E/\hat{b})^{\rho}}{1+(E/\hat{a})^{\sigma}}. \tag{5.2}$$

The fitting parameters in (5.1) are the power-law exponents δ, σ, ρ and amplitudes $\hat{y}, \hat{a}, \hat{b}$, as well as the exponent $\hat{\beta} = 1/(k_{\rm B}T)$ determining the cutoff. The ultra-relativistic limit applies, since the fit is done above a cutoff energy $E_{\rm cut}$ where $m^2/E^2 \ll 1$. (We use $E_{\rm cut} \approx 1$ on the GeV scale.) In this limit, the mass-square m^2 is not a fitting parameter, as it is absorbed in the amplitudes $\hat{y}, \hat{a}, \hat{b}$. The classical spectral particle density reads, cf. (4.4) and (4.12),

$$\frac{\mathrm{d}\rho_{\rm B}}{\mathrm{d}E}(\mathrm{GeV}^{-1}\ \mathrm{m}^{-3}) \sim \frac{4\pi}{c}\hat{y}f_{\rm B}(E)E^{2-\delta}\ \mathrm{e}^{-\hat{\beta}E}\sqrt{1-\frac{m^2}{E^2}}. \tag{5.3}$$

The root can be dropped in the ultra-relativistic regime, and $\hat{y} = cs\hat{z}/(2\pi\hbar c)^3$, cf. (4.2), (4.8) and (4.11). The spin multiplicity is $s = 2$.

The electron flux $F_{\rm e}(E)$ in Fig. 1 is fitted with

$$E^3F_{\rm e}(E) = 39.0E^{5-3.0}\frac{1+(E/100)^{1.0}}{1+(E/2.87)^{2.4}}\exp(-1.0\times10^{-3}E). \tag{5.4}$$

The parameters in (5.1) and (5.2) can be read off from this equation. The positron fraction $R_{\rm p}(E) = F_{\rm p}/(F_{\rm e}+F_{\rm p})$, where $F_{\rm p}(E)$ denotes the positronic flux density, was measured by the AMS Collaboration [23], cf. Fig. 3, without disentangling the electron and positron flux, and an analytic fit of the positron fraction was derived,

$$R_{\rm p}^{\rm AMS}(E) = \frac{0.091E^{-0.63}+0.0078E^{0.66}\ \mathrm{e}^{-0.0013E}}{1+0.091E^{-0.63}+2\times0.0078E^{0.66}\ \mathrm{e}^{-0.0013E}}, \tag{5.5}$$

where E is in GeV units. Combining the electronic flux density (5.4) with the AMS ratio (5.5), we find an analytic representation of the positron flux,

$$F_{\rm p}^{\rm AMS}(E) = F_{\rm e}(E)\frac{R_{\rm p}^{\rm AMS}(E)}{1-R_{\rm p}^{\rm AMS}(E)}. \tag{5.6}$$

In Fig. 2, we approximate this analytic function by a power-law density $F_{\rm p}(E)$ of the form (5.1),

$$E^3F_{\rm p}(E) = 4.0E^{5-3.5}\frac{1+(E/18.5)^{1.3}}{1+(E/2.74)^{2.1}}\exp(-1.35\times10^{-3}E). \tag{5.7}$$

This is a power-law fit to $E^3F_{\rm p}^{\rm AMS}(E)$ as defined by (5.6) with $F_{\rm e}(E)$ in (5.4) and $R_{\rm p}^{\rm AMS}(E)$ in (5.5). In Fig. 3, we plot the positron fraction $R_{\rm p}(E) = F_{\rm p}/(F_{\rm e}+F_{\rm p})$, now directly calculated with the electronic/positronic power-law densities $F_{\rm e}(E)$ in (5.4) and $F_{\rm p}(E)$ in (5.7), and compare it to the analytic fit $R_{\rm p}^{\rm AMS}(E)$ of the AMS data in (5.5). The thermodynamic parameters of the nonthermal electron–positron plasma are listed in Table 1, extracted from the flux densities $F_{\rm e,p}(E)$ in (5.4) and (5.7).

6. Conclusion

The goal is to find power-law densities suitable for ultra-relativistic wideband fitting. A consistent thermodynamic formalism requires these distributions to admit an extensive and stable entropy functional resulting in thermodynamic variables with positive standard deviations and relative fluctuations vanishing in the thermodynamic limit. Here, we have discussed a class of stable power-law densities, stationary non-equilibrium distributions defined by an empirical spectral function, a power-law ratio to be inferred from measured flux densities, cf. Sections 2 and 3.

We explained the spectral fitting with ultra-relativistic power-law densities, cf. Section 4, and applied it to cosmic-ray electrons treated as dilute nonthermal plasma, cf. Section 5. The cosmic-ray electron flux as well as the AMS and PAMELA positron fraction [23,24] are highly isotropic. The statistical description given here does not involve any hypothetical assumptions on isotropically distributed electron/positron sources and production mechanisms. The power-law densities are empirically determined from spectral fits [25–28].

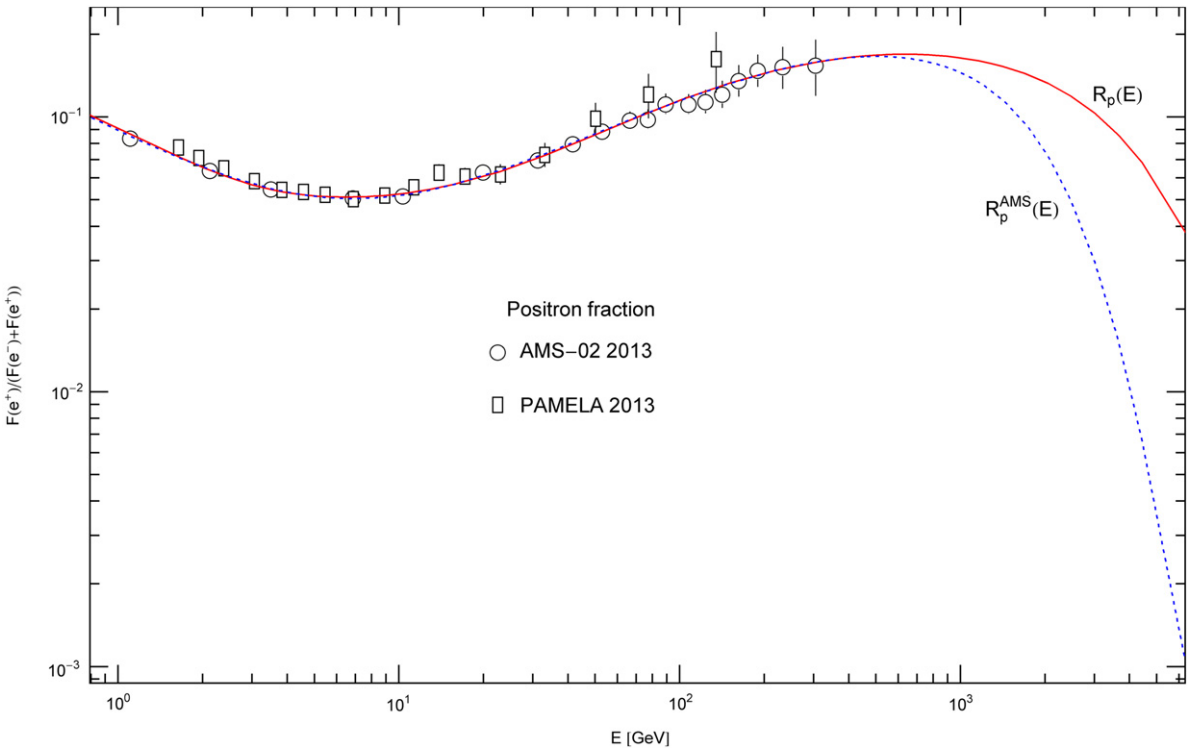

Fig. 3. Positron fraction. Data points from AMS-02 2013 (Alpha Magnetic Spectrometer) [23] and PAMELA 2013 [24]. The dotted curve depicts the analytic fit $R_p^{AMS}(E)$ obtained in Ref. [23], cf. (5.5). Above 300 GeV, $R_p^{AMS}(E)$ is an analytic extrapolation, a plot of the AMS ratio (5.5). The solid curve $R_p(E)$ is the positron fraction $F_p/(F_e+F_p)$ calculated from the electron flux $F_e(E)$ in (5.4) (obtained from the fit in Fig. 1) and the positron flux $F_p(E)$ in (5.7). The latter is found by approximating the AMS flux $F_p^{AMS}(E)$ below 300 GeV by a nonthermal classical power-law density, cf. Fig. 2. The depicted exponential decay of the analytic AMS fraction $R_p^{AMS}(E)$ is intermediate, terminating at about 10 TeV (with subsequent power-law decay according to (5.5)), in contrast to the predicted positron fraction $R_p(E)=F_p/(F_e+F_p)$, whose exponential decay is final, determined by the temperature of the electron/positron flux densities in (5.4) and (5.7).

Cosmic-ray electrons/positrons constitute a dilute nonthermal two-component plasma, whose components can efficiently be modeled as classical ultra-relativistic power-law ensembles. The classical limit allows fairly explicit evaluation of the thermodynamic functions in (T, N, V) representation. High-temperature expansions are not efficient though, as they cannot adequately describe peak-to-peak cross-overs in wideband spectra. The electron and positron spectra in Figs. 1 and 2 are not wideband, extending from the low GeV to the low TeV region, but there are still two spectral peaks discernible, and the cross-over is beyond asymptotic expansions.

The cosmic-ray electron spectrum is well covered by several measurements in the GeV and low TeV range. Once the power-law fit of the spectral electron density is performed, cf. Fig. 1, it can be combined with the measured positron fraction, cf. Fig. 3, to obtain an estimate of the positronic flux density [24,29]. The positron flux is modeled by a nonthermal power-law density composed of two spectral peaks like the electronic counterpart, cf. Fig. 2. The thermodynamic parameters of the electron/positron gas can be read off from the spectral fits. The temperature of the two non-equilibrated components is comparable but decidedly different, and their specific energy, entropy and number densities differ by roughly one order, cf. Table 1.

References

[1] D. Band, et al., Astrophys. J. 413 (1993) 281.
[2] R.D. Preece, et al., Astrophys. J. Suppl. 126 (2000) 19.
[3] N.M. Lloyd, V. Petrosian, Astrophys. J. 543 (2000) 722.
[4] N.A. Hussein, D.A. Eisa, M.G. Eldin, Physica A 391 (2012) 6690.
[5] X.-J. Wen, Physica A 392 (2013) 4388.
[6] O. Adriani, et al., Phys. Rev. Lett. 106 (2011) 201101.
[7] M. Ackermann, et al., Phys. Rev. Lett. 108 (2012) 011103.
[8] M. Ackermann, et al., Phys. Rev. D 82 (2010) 092004.
[9] A. Razdan, Physica A 392 (2013) 982.
[10] F. Aharonian, et al., Astron. Astrophys. 508 (2009) 561.
[11] F. Aharonian, et al., Phys. Rev. Lett. 101 (2008) 261104.
[12] R. Tomaschitz, Physica A 385 (2007) 558.
[13] R. Tomaschitz, Physica A 387 (2008) 3480.

[14] R. Tomaschitz, Physica B 405 (2010) 1022.
[15] R. Tomaschitz, Phys. Lett. A 372 (2008) 4344.
[16] R. Tomaschitz, Phys. Lett. A (2013) http://dx.doi.org/10.1016/j.physleta.2013.10.016.
[17] R. Tomaschitz, Physica A 307 (2002) 375.
[18] D.V. Anghel, A.S. Parvan, A.S. Khvorostukhin, Physica A 391 (2012) 2313.
[19] J.M.B. Noronha, D.J. Toms, Physica A 392 (2013) 3984.
[20] S.G. Brush, H.L. Sahlin, E. Teller, J. Chem. Phys. 45 (1966) 2102.
[21] S. Ichimaru, Rev. Mod. Phys. 54 (1982) 1017.
[22] S. Ichimaru, H. Iyetomi, S. Tanaka, Phys. Rep. 149 (1987) 91.
[23] M. Aguilar, et al., Phys. Rev. Lett. 110 (2013) 141102.
[24] O. Adriani, et al., Phys. Rev. Lett. 111 (2013) 081102.
[25] R. Tomaschitz, Astropart. Phys. 27 (2007) 92.
[26] R. Tomaschitz, EPL 89 (2010) 39002.
[27] R. Tomaschitz, Opt. Commun. 282 (2009) 1710.
[28] R. Tomaschitz, Physica B 404 (2009) 1383.
[29] M.A. DuVernois, et al., Astrophys. J. 559 (2001) 296.